S1 Calculated phase diagram and Crystal structure

Figure S1 shows the calculated Li-Fe-P phase diagram[1] equilibrated with an oxygen potential under reducing conditions. The diagram indicates how different off-stoichiometry conditions lead to different secondary phases. Following the 'A' direction in the diagram, poorly crystallized lithium phosphates which are good lithium conductors can be introduced, whereas the more typical Li excess (B direction) or Li-deficiency (C direction) lead to Fe-oxides or Fe-phosphates. Figure S2 shows the XRD pattern for the off-stoichiometric material synthesized at 600°C under Ar gas. The crystalline component of the material is clearly $LiFePO_4$ with no impurity peaks present.

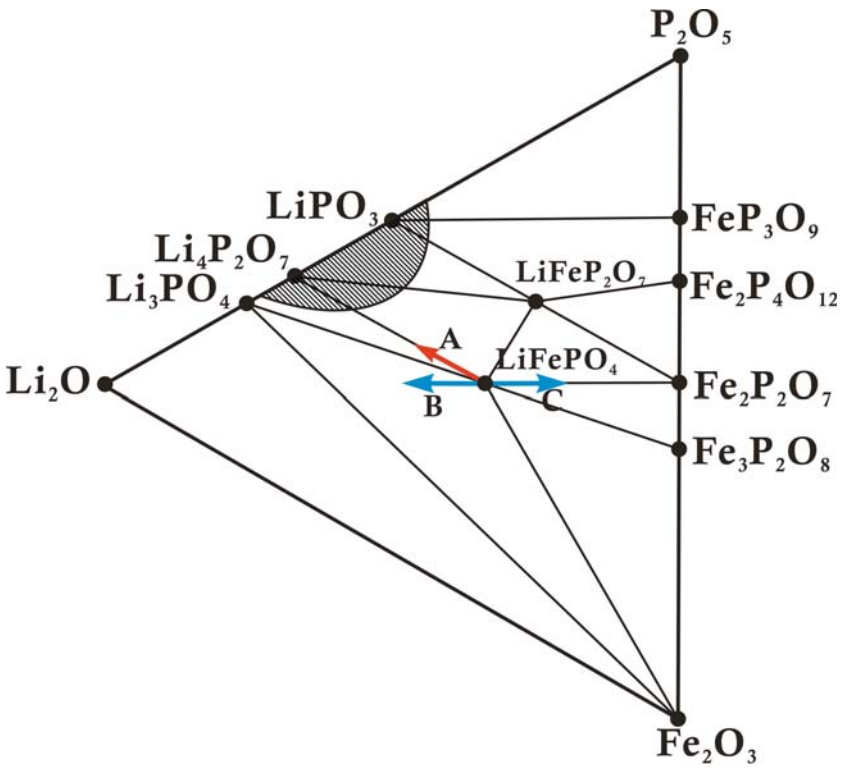

Figure S1. **Calculated Li-Fe-P ternary phase diagram equilibrated with an oxygen potential under reducing conditions.** The 'A' arrow indicates off-stoichiometry induced in the samples described in this Letter. The 'B' and 'C' arrow respectively indicate the more common one-to-one Fe/P deficiency and lithium deficiency. The shaded area in phase diagram indicates relevant coating compositions.

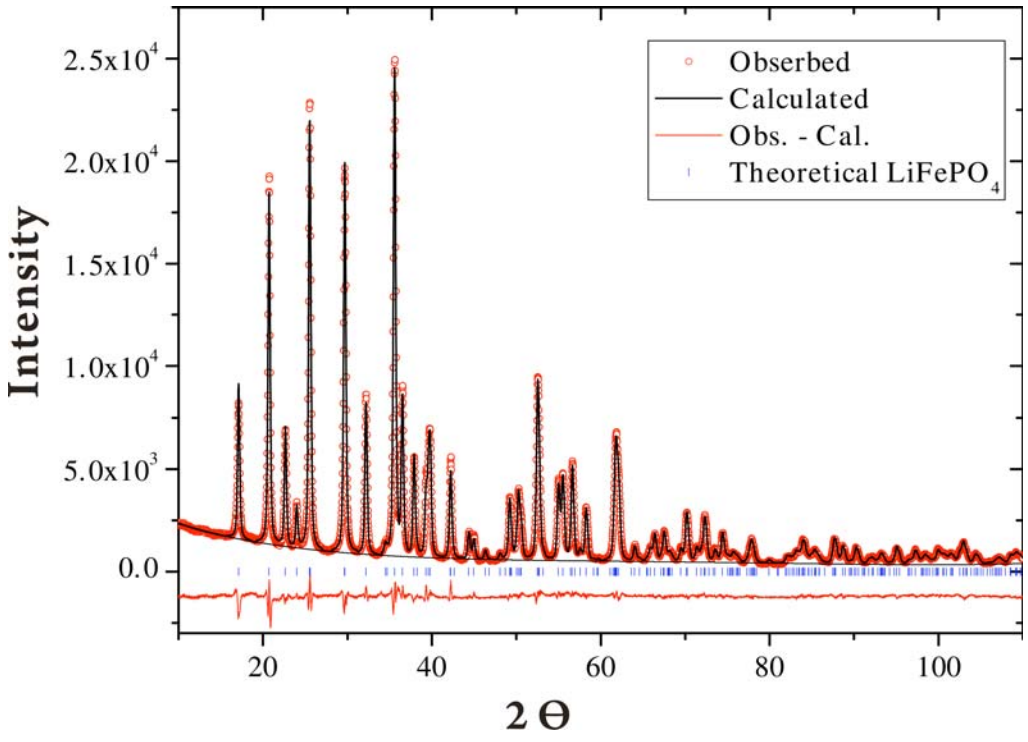

Figure S2. The Rietveld refinement result for $LiFe_{0.9}P_{0.95}O_{4-\delta}$ synthesized at 600˚C under Ar. The R_{wp} is 5.677 and the R_p is 2.458. Lattice constants of olivine structure are 10.3134 ±0.000255 (Å), 6.002 ±0.000151 (Å), 4.691 ±0.000128 (Å), respectively a, b, c. The crystallite size is 32.4 nm (From X'pert High Score plus software)

S2 Characterization of the Second Phase Coating Material

We believe that the second phase coating is a poorly crystallized pyrophosphate which contains some amount of Fe^{3+}. We base this on several independent measurement techniques. The **STEM** analysis in Figure S3-1 shows a lower Fe/P ratio in the surface than in the inside of the grain. This measurement was repeated at three different places of the sample with similar results. In contrast, the stoichiometric sample does not show this effect with a similar Fe/P ratio on the surface and in the bulk in Figure S3-2. **XPS** analysis for our materials shows two different P chemical states. One is close to P 2p in $LiFePO_4$ and the other is close to P 2p in $Li_4P_2O_7$ in Table S1. We have received independent verification of this from **NMR** (data not shown) which indicates the presence of a diamagnetic P_2O_7 environment in the sample[2]

Figure S4-1 shows the **Mössbauer** spectrum of our sample at room temperature. Besides the typical IS and QS observed for Fe^{2+} in $LiFePO_4$ the spectrum shows additional peaks. To investigate whether these peaks come from Fe_2P we repeated the Mössbauer at 77.3 K where Fe_2P is expected to be ferromagnetic which creates several extra peaks, but besides minor shifts of the peak positions, no changes were observed (data not shown). FeP on the other hand is antiferromagnetic[3] and cannot be detected in this way. Figure S4-2 shows a map of the IS and QS of the extra peaks in our sample, as well as data available in the literature for Fe in various environments. This comparison leads us to conclude that Fe^{3+} is likely to be present in the poorly crystallized pyrophosphate in our material. Indeed, it is well known from previous literature that amorphous Li-pyrophosphates are good glass formers and can have substantial 3d transition metal content[4,5,6].

To further confirm the presence of Fe^{3+} in our sample we tested an as-made sample for **initial discharge capacity** and found that it had about 20 mAh/g initial discharge in Figure S5. This Fe^{3+} capacity was fully reversible over many cycles. Hence, we believe that Fe^{3+} in the poorly crystallized pyrophosphate coating is electrochemically active and contributes to the low voltage capacity tail that can be observed in our discharge profiles.

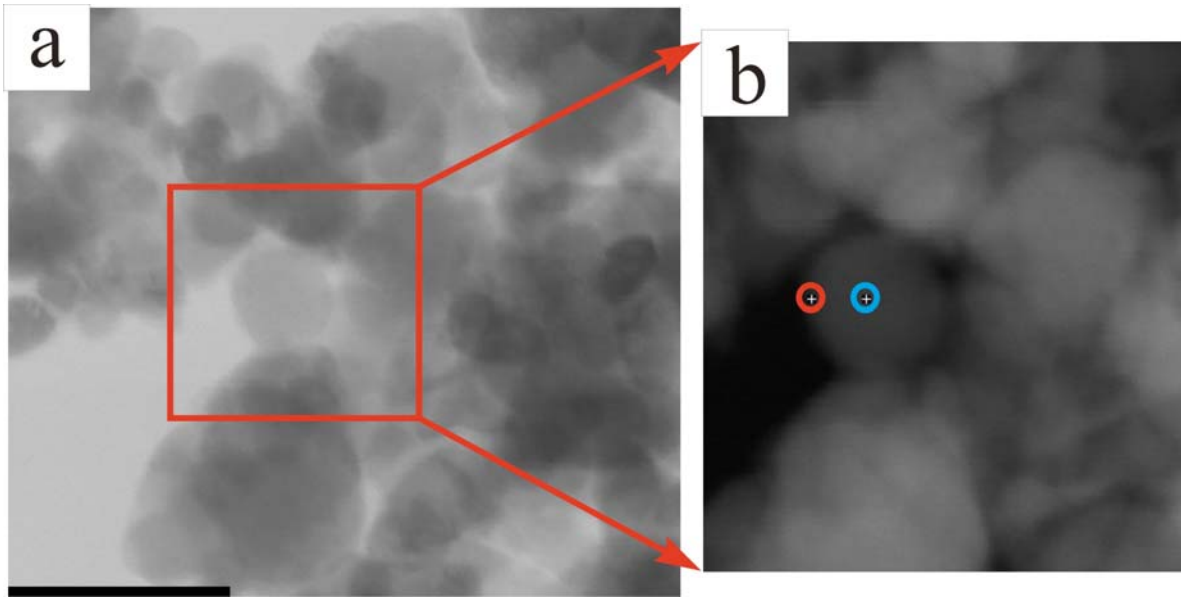

(c)

	Region 1	Region 2	Region 3
Fe/P ratio in the inside of grain	0.9	0.86	0.84
Fe/P ratio in the surface	0.67	0.68	0.65

Figure S3-1. Point elemental analysis data from STEM measurement for $LiFe_{0.9}P_{0.95}O_{4-\delta}$ synthesized at 600˚C under Ar. (a) STEM bright field image, (b) STEM dark field image at region (a). Red circle indicates where the surface measurement is taken, and the blue circle represents the measurement in the inside of the grain. This measurement was repeated at two additional regions of the sample. The result for all three regions is given in (c). Scale bar is 100 nm.

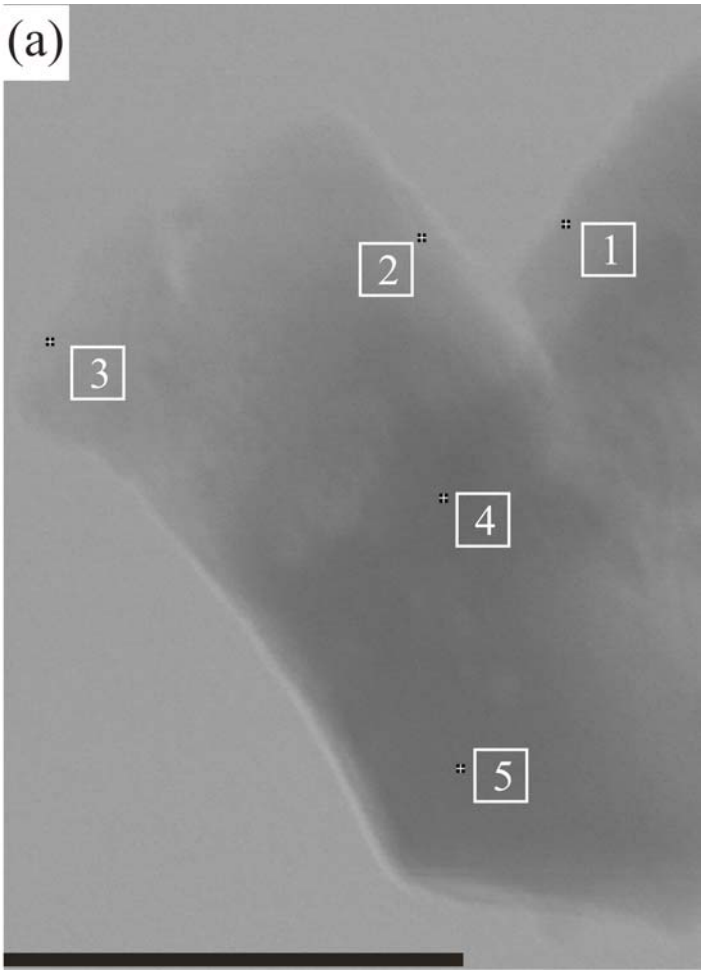

(b)

Region	Fe	P	Fe/P ratio
1	23.60151	22.18518	1.06
2	24.23624	20.06235	1.20
3	22.61357	22.24539	1.01
4	23.7964	21.70314	1.096
5	23.86865	20.7388	1.150

Figure S3-2. Point elemental analysis data from STEM measurement for $LiFePO_4$ synthesized at 600˚C under Ar. (a) STEM data for stoichiometric $LiFePO_4$ synthesized at 600°C. (b) The ratio of iron to phosphorus (Fe/P) from STEM point analysis at different regions for $LiFePO_4$ synthesized at 600˚C. Scale bar is 100nm

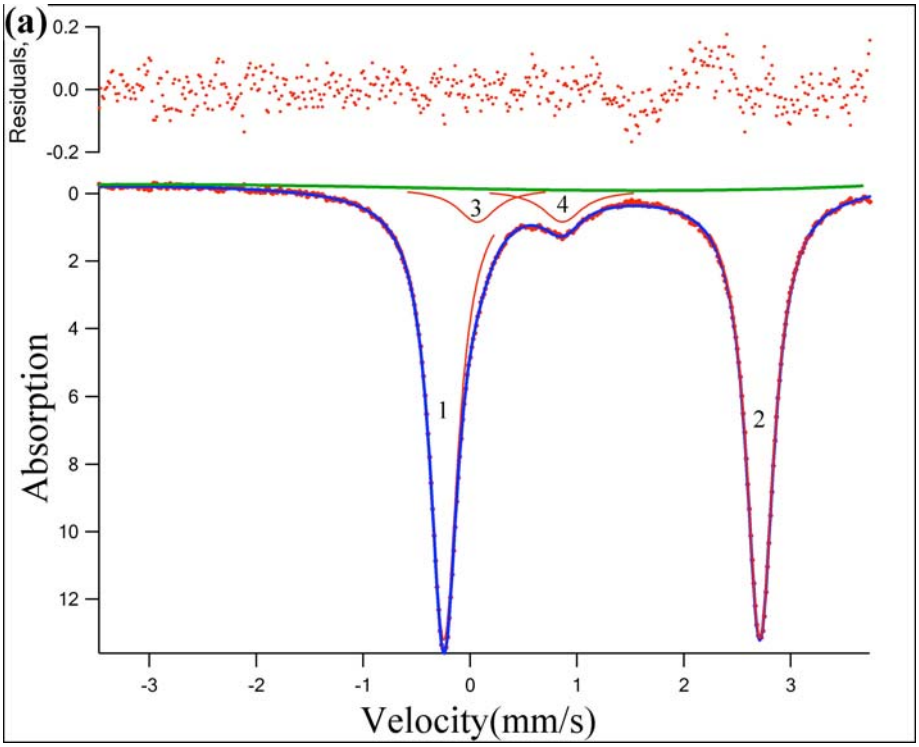

(b)

	δ(IS)	Δ(QS)	Γ (FWHM)	Weight percentage
1, 2 (Fe^{2+} in $LiFePO_4$)	1.2327	2.956	0.31	90.7
3, 4	0.464	0.7986	0.44	9.3

Figure S4-1. Mössbauer spectroscopy data and fitted data based on Lorentzian shape for $LiFe_{0.9}P_{0.95}O_{4-\delta}$ synthesized at 600°C. The measurement was performed **at 293K**. The value is relative to iron metal foil. Solid dot: observed data. Blue solid line: fitted $LiFePO_4$ Red solid line: fitted data for different iron environment. Our material has two different iron environments. One is Fe^{2+} in $LiFePO_4$. Based on literature data available for inorganic phosphate glass[5] (Figure S4-2), we assign the other environment to Fe^{3+} in octahedral sites in the poorly crystallized pyrophosphate environment.

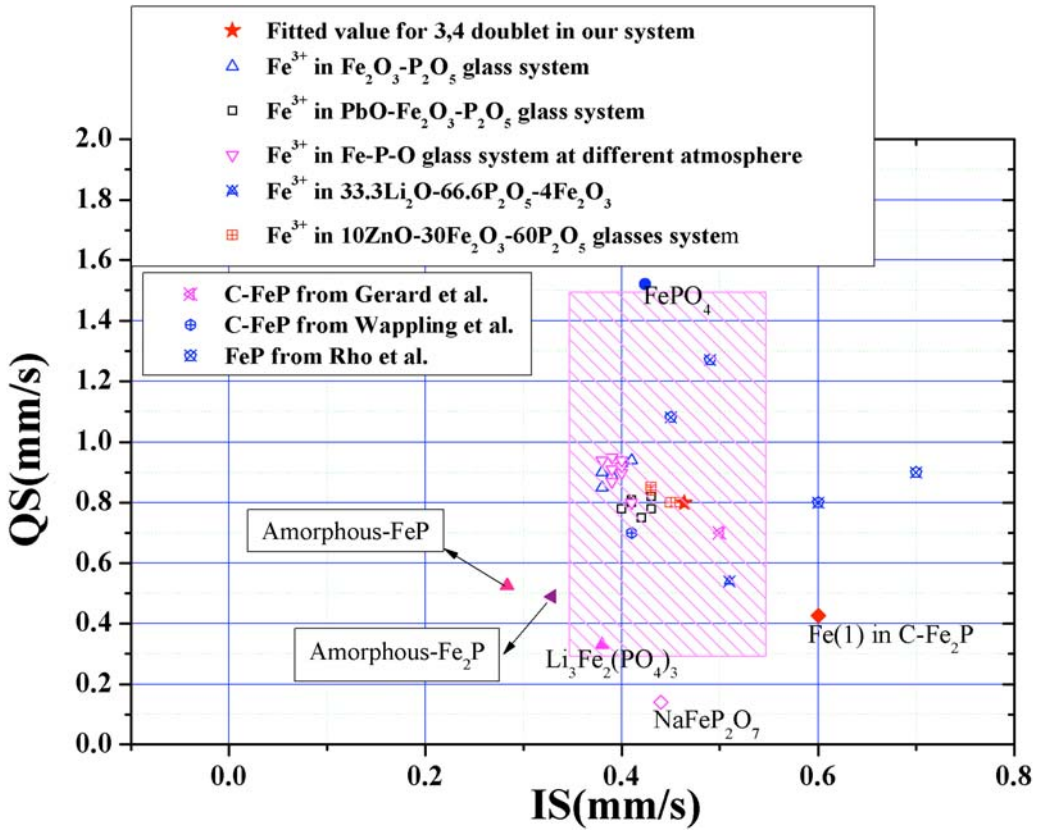

Figure S4-2. A map of the value of IS and QS in several crystalline systems and inorganic glass systems at room temperature[7,8,9,10,11,12,13,14,15,16,17,18,19,20]. The shaded region represents the IS and QS value of Fe^{3+} in octahedral site in inorganic glasses system[9]. The red star represents on the IS and QS for the 3, 4 doublet in Figure S4-1, which is associated with the non-$LiFePO_4$ phase. The value of IS and QS is close to that typically found for Fe^{3+} in octahedral site in inorganic glasses, especially with P_2O_7 structure[17]. IS and QS values of FeP also fall into the shaded region[8,20].

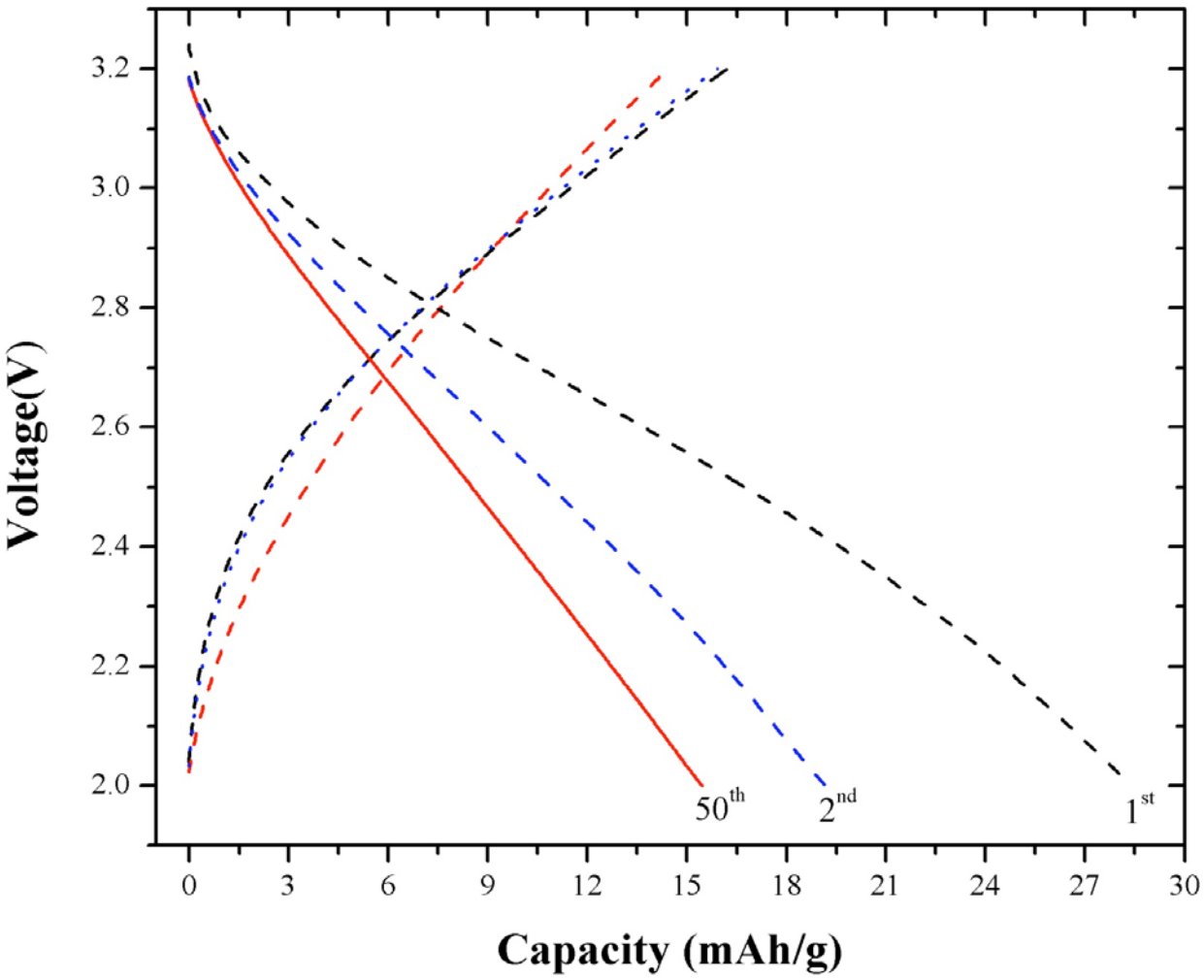

Figure S5. Electrochemical voltage profile between 3.2V and 2.0V for a cell started in discharge with as-made $LiFe_{0.9}P_{0.95}O_{4-\delta}$ synthesized at 600°C. The rate was C/30 based on $LiFePO_4$, which has 170 mA/g at 1C. This confirms that the Fe^{3+} in the amorphous pyrophosphate coating is electrochemically active and can contribute to the capacity at low voltage. The loading density was 2.93 mg/cm^2. The electrode was composed of active material (80), carbon (15), and binder (5) (weight percentage).

Samples	P $2p_{3/2}$	P $2p_{1/2}$	P $2p_{3/2}$	P $2p_{1/2}$	Δ* (eV)	FWHM (eV)	Area Ratio*	Area %
	P 2p doublet for $LiFePO_4$ (eV)		P 2p doublet for $Li_4P_2O_7$ (eV)					
$LiFePO_4$	133.38	134.22	N/A		0.84	1.17	1:2	100:0
$LiFe_{0.9}P_{0.95}O_{4-\delta}$	133.36	134.20	133.80	134.64	0.84	1.16/1.25	1:2	81:19
$Li_4P_2O_7$	N/A		133.63	134.47	0.84	1.22	1:2	0:100

Table S1. Fitted values of peak position based on P 2p doublet for $LiFePO_4$, $LiFe_{0.9}P_{0.95}O_{4-\delta}$, and $Li_4P_2O_7$. The line shape of peak for fitting is the product of a Gaussian (0.7) and a Lorentzian (0.3). The peak position, FWHM, and the area of P $2p_{3/2}$ peak were fitted by using CasaXPS software. The parameters of P $2p_{1/2}$ peak were made to depend on those of P $2p_{3/2}$ peak by a constant shift Δ and fixed ratio of integrated intensity. $LiFe_{0.9}P_{0.95}O_{4-\delta}$ shows two different P chemical states. One is close to P 2p in $LiFePO_4$ and the other is close to P 2p in $Li_4P_2O_7$. The ratio of integrated intensities of the two chemical states is 81: 19. The data was corrected by the binding energy of the adventitious hydrocarbon, C 1s = 248.8 eV[21].

S3 Control experiments on stoichiometric $LiFePO_4$

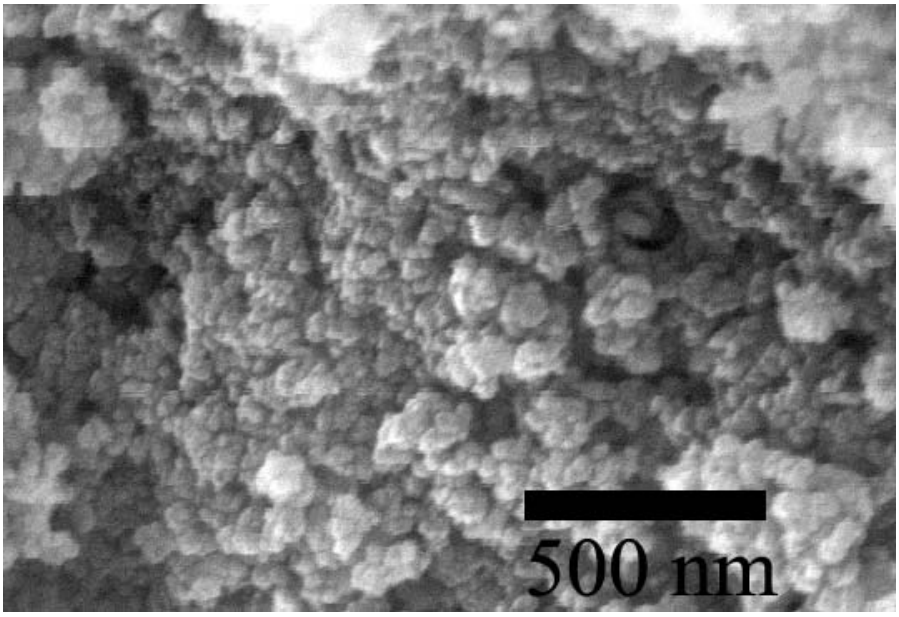

(a)

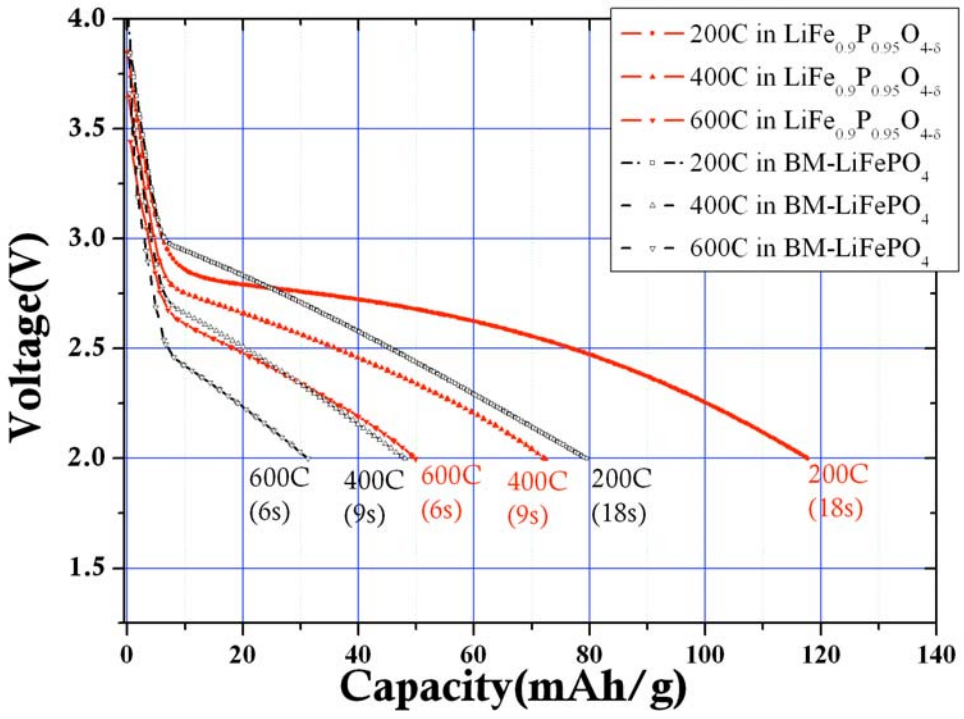

(b)

Figure S6. (a) SEM image for $LiFePO_4$ obtained with the same synthesis procedure as the off-stichiometric material but with ball milled precursors. The particle size is less than 50nm. Rietveld analysis on the XRD pattern of stoichiometric $LiFePO_4$ indicated a particle size of 32nm which is comparable to that of $LiFe_{0.9}P_{0.95}O_{4-\delta}$. Without ball milling of the precursors the particle size of stoichiometric $LiFePO_4$ is larger than that of $LiFe_{0.9}P_{0.95}O_{4-\delta}$ as the coating phase in the off-stoichiometric material probably reduces grain growth. (b) Discharge at various rates for ball-milled $LiFePO_4$ and $LiFe_{0.9}P_{0.95}O_{4-\delta}$ with similar particle size. The cells were charged at C/2 and held at 4.3V until the current reaches C/20. The loading density was 3.18 mg/cm^2 for $LiFe_{0.9}P_{0.95}O_{4-\delta}$ and 3.11 mg/cm^2 for $LiFePO_4$. The formulation of electrode is 30 (active): 65 (carbon): 5 (binder) in wt %.

S4 Methods

XRD Measurement

The X-ray pattern was obtained on a Rigaku diffractometer with Cu-Kα radiation, and was slowly scanned at 1˚/5s over a 2θ range from 10˚ to 110˚ at step mode. The lattice parameters were determined by Rietveld refinement analysis using the X'pert High Score Plus software.

TEM Measurement

TEM (Transmission Electron Microscopy) images were collected from the powder sample which was dispersed in isopropanol, and suspended on a carbon support film with copper grid under an accelerating voltage of 200 KV on a JEOL 2010 microscope.

STEM Measurement

STEM (Scanning Transmission Electron Microscopy) images were collected from the powder sample which was dispersed in methanol, and suspended on a carbon support film with copper grid under accelerating voltage of 250 KV on VG HB603 FEG-STEM. Beam resolution is around 2nm.

SEM Measurement

SEM (Scanning Electron Microscopy) measurement was performed on a FEI/Philips XL30 FEG ESEM. The samples on the stainless holder with double-sided carbon tape were coated with gold/palladium.

XPS Measurement

XPS (X-Ray photoelectron Spectroscopy) analysis was performed using a Kratos AXIS Ultra Imaging XPS equipped with a monochromatic Al (1486.6 eV) X-ray source. The pass energy was 20 eV and step size 100 meV. The powder samples were mounted on stainless holder with double-sided carbon tape and copper tape. The chamber was maintained at a pressure of less than 10^{-9} mbar. The analysis of the data was performed with CasaXP VAMAS processing software. All data have been referenced by adventitious hydrocarbon

binding energy (C 1S =284.8 eV[21]). The data were corrected with Relative Sensitivity Factors (RSF) provided by our spectrometer. Relative sensitivity factors (RSF) for P 2p and Fe 2p was given as 0.486 and 2.957, respectively.

Mössbauer Spectroscopy measurement

The Mössbauer spectra were determined using a conventional constant acceleration spectrometer operated in multi-channel scaling mode. The gamma ray source consisted of 119 mCi of Co^{57} in a rhodium metal matrix that was maintained at ambient temperature. The spectrometer was calibrated using a 6-micron thick natural abundance iron foil. Isomer shifts are reported relative to the center of the magnetic hyperfine pattern of the latter foil (at ambient temperature) taken as zero velocity. The line widths of the inner-most pair of $\Delta M_I = \pm 1$ transitions of the latter Zeeman pattern were reproducibly determined to be 0.214 mm/s. The measurement was performed at 293K.

Refereces

1 Ong, S. P., Wang, L., Kang, B. & Ceder, G. Li-Fe-P-O-2 phase diagram from first principles calculations. *Chemistry of Materials* **20**, 1798-1807 (2008).

2 Private communication with Prof. C. Grey and Dr. J. Shirakawa for NMR data.

3 Häggstrom, L. & Narayanasamy, A. Mössbauer study of the magnetic-structure of FeP. *J. Magn. Magn. Mater.* **30**, 249-256 (1982).

4 Sobha, K. C. & Rao, K. J. Investigation of phosphate glasses with the general formula $A_xB_yP_3O_{12}$ where A=Li, Na or K and B=Fe, Ga, Ti, Ge, V or Nb. *Journal of Non-Crystalline Solids* **201**, 52-65 (1996).

5 Sayer, M. & Mansingh, A. Transport properties of semiconducting phosphate glasses. *Physical Review B* **6**, 4629-4643 (1972).

6 Martin, S. W. & Angell, C. A. DC and AC conductivity in wide composition range Li_2O---P_2O_5 glasses. *Journal of Non-Crystalline Solids* **83**, 185-207 (1986).

7 Bailey, R. E. & Duncan, J. F. Mössbauer and nuclear magnetic resonance studies of several iron phosphides. *Inorg. Chem.* **6**, 1444-1447 (1967).

8 Wäppling, R., Häggstrom, L., Rundqvist, S. & Karlsson, E. Mössbauer study of phosphides containing iron. *Journal of Solid State Chemistry* **3**, 276-292 (1971).

9 Dyar, M. D. A review of Mössbauer data on inogrganic glasses- The effects of composition on iron valency and coordination. *American Mineralogist* **70**, 304-316 (1985).

10 McCally, R. L., Morgan, J. S., Kistenmacher, T. J. & Moorjani, K. Local atomic-structure in amorphous Fe-P alloys. *Journal of Applied Physics* **63**, 4124-4126 (1988).

11 Mercader, R. C. *et al.* Mössbauer effect, magnetic, and neutron-diffraction study of $NaFeP_2O_7$. *Physical Review B* **42**, 25-32 (1990).

12 Elsukov, E. P., Vorobev, Y. N. & Trubachev, A. V. Local atomic structure and hyperfine interactions in electrodeposited $Fe_{100-x}P_x$ ($18 < x < 45$) alloys. *Physica Status Solidi (a)* **127**, 215-222 (1991).

13 Marasinghe, G. K. *et al.* Structural features of iron phosphate glasses. *Journal of Non-Crystalline Solids* **222**, 144-152 (1997).

14 Mogus-Milankovic, A., Rajic, M., Drasner, A., Trojko, R. & Day, D. E. Crystallisation of iron phosphate glasses. *Physics and Chemistry of Glasses* **39**, 70-75 (1998).

15 Goni, A. *et al.* Spectroscopic and magnetic properties of α-$Li_3Fe_2(PO_4)_3$: A two-sublattice ferrimagnet. *Chemistry of Materials* **12**, 62-66 (2000).

[16] Mogus-Milankovic, A. M., Santic, A., Reis, S. T., Furic, K. & Day, D. E. Studies of lead-iron phosphate glasses by Raman, Mössbauer and impedance spectroscopy. *Journal of Non-Crystalline Solids* **351**, 3246-3258 (2005).

[17] Reis, S. T. *et al.* Iron redox equilibrium, structure and properties of zinc iron phosphate glasses. *Journal of Non-Crystalline Solids* **353**, 151-158 (2007).

[18] Kashif, I., Rahman, S. A., Mostafa, A. G., Ibrahim, E. M. & Sanad, A. M. Structural analysis and physical properties of iron-molybdenum lithium-borate glasses. *Journal of Alloys and Compounds* **450**, 352-358 (2008).

[19] Almeida, A. F. L., Vasconcelos, I. F., Valente, M. A. & Sombra, A. S. B. The optical and ^{57}Fe Mössbauer spectra of lithium diborate ($Li_4B_2O_7$) in borophosphate glass-ceramics. *Physica B: Condensed Matter* **322**, 276-288 (2002).

[20] Rho, Y. H., Nazar, L. F., Perry, L. & Ryan, D. Surface chemistry of $LiFePO_4$ studied by Mössbauer and X-ray photoelectron spectroscopy and its effect on electrochemical properties. *Journal of the Electrochemical Society* **154**, A283-A289 (2007).

[21] Moulder, J. F., Stickle, W. F., Sobol, P. E. & Bomben, K. D. *Handbook of X-ray Photoelectron Spectroscopy: A reference book of standard spectra for identification and interpretation of XPS data*. (Physical Electronics, Inc., 1995).